

# Understanding the property of $\eta(1405/1475)$ in the $J/\psi$ radiative decay

Xiao-Gang Wu<sup>1</sup>, Jia-Jun Wu<sup>1,2</sup>, Qiang Zhao<sup>1\*</sup>, and Bing-Song Zou<sup>1,3†</sup>

1) *Theoretical Physics Center for Science Facilities, Institute of High Energy Physics, Chinese Academy of Sciences, Beijing 100049, China*

2) *Physics Division, Argonne National Laboratory, Argonne, Illinois 60439, USA*

3) *State Key Laboratory of Theoretical Physics, Institute of Theoretical Physics, Chinese Academy of Sciences, Beijing 100190, China*

(Dated: June 8, 2018)

In this work we make a systematic analysis of the correlated processes  $J/\psi \rightarrow \gamma\eta(1440)/f_1(1420)$  with  $\eta(1440)/f_1(1420) \rightarrow K\bar{K}\pi$ ,  $\eta\pi\pi$  and  $3\pi$ , where the role played by the so-called “triangle singularity mechanism” (TSM) is clarified. Our results agree well with the experimental data and suggest a small fraction of  $f_1(1420)$  contributions in these processes. This study confirms our conclusion in [Phys. Rev. Lett. 108, 081803 (2012)] that the dynamic feature of the TSM can be recognized by the strong narrow peak observed in the  $\pi\pi$  invariant mass spectrum of  $\eta(1440) \rightarrow 3\pi$  with anomalously large isospin violations. Nevertheless, we explicitly demonstrate that the TSM can produce obvious peak position shifts for the same  $\eta(1440)$  or  $f_1(1420)$  state in different decay channels. This is a strong evidence that the  $\eta(1405)$  and  $\eta(1475)$  are actually the same state, i.e.  $\eta(1440)$ . We also make an analysis of the radiative decays of  $\eta(1440) \rightarrow \gamma V$  ( $V = \phi, \rho^0$  or  $\omega$ ) which shows that such a one-state prescription seems not to have a conflict with the so-far existing experimental data. Our analysis may shed a light on the long-standing puzzling question on the nature of  $\eta(1405)$  and  $\eta(1475)$ .

PACS numbers: 13.75.Lb, 14.40.Rt, 13.20.Gd

## I. INTRODUCTION

The charmonium hadronic and radiative decays into light hadrons have provided an important way to probe the light hadron structures. In particular, with high statistics of  $J/\psi$  and  $\psi'$  events produced in  $e^+e^-$  annihilation, the light hadron spectra can be studied closely and dynamic information concerning the light hadron properties can be extracted from their production and decays. During the past few years, there have been several new resonance structures with  $J^{PC} = 0^{-+}$  observed by BESII and BESIII in  $J/\psi$  and  $\psi'$  decays. They could be candidates of radial excitation states of the pseudoscalar mesons  $\eta$  and  $\eta'$ , or exotic states such as glueball, multi-quark state or hadronic molecule. For instance, the BES-II Collaboration first reported a resonance structure in  $J/\psi \rightarrow \gamma X(1835) \rightarrow \gamma\eta'\pi^+\pi^-$  [1], which was later confirmed by the BESIII measurement [2] with high statistics. Nevertheless, two additional resonance structures were identified as  $X(2120)$  and  $X(2370)$  in the  $\eta'\pi\pi$  invariant mass spectrum [2, 3].

In fact, our understanding of the isoscalar spectrum is still far from well-established. Historically, the study of the nature of  $\eta(1405)$  and  $\eta(1475)$  has been a hot topic and closely related to the effort of searching for the ground state pseudoscalar glueball in experiment. Since the first radial excitation states of  $\eta$  and  $\eta'$  are generally assigned to  $\eta(1295)$  and  $\eta(1475)$  taking into account their production and decay properties [4], it leaves out the abundant  $\eta(1405)$  as a possible candidate for the pseudoscalar glueball. However, we would like to emphasize that such an arrangement still needs further studies, and it is still controversial whether  $\eta(1405)$  and  $\eta(1475)$  are two separated states or just one state of  $0^{-+}$  in different decay modes [5].

With the availability of high-statistic  $J/\psi$  and  $\psi'$  events from the BESIII Collaboration, it allows us to tackle the question on the nature of  $\eta(1405)$  and  $\eta(1475)$ . One important experimental progress is that the BESIII Collaboration [6] report the observation of anomalously large isospin violations of the  $\eta(1405/1475) \rightarrow 3\pi$  in  $J/\psi \rightarrow \gamma\eta(1405/1475) \rightarrow \gamma\pi^0 f_0(980) \rightarrow \gamma + 3\pi$  which, however, can hardly be understood by treating them as either glueball or  $q\bar{q}$  state. Interestingly, this decay process also explicitly involves the issue of  $a_0(980)$ - $f_0(980)$  mixings. The BESIII data show that the  $f_0(980)$  signal is only about 10 MeV in width and the lineshape is different from the Breit-Wigner width of about  $40 \sim 100$  MeV [4]. Moreover, the isospin violation turns out to be significant with  $BR(\eta(1405) \rightarrow f_0(980)\pi^0 \rightarrow 3\pi)/BR(\eta(1405) \rightarrow a_0^0(980)\pi^0 \rightarrow \eta\pi\pi) = (17.9 \pm 4.2)\%$ , which cannot be explained by the  $a_0 - f_0$  mixing intensity measured in other channels [7].

An immediate theoretical interpretation is given by Ref. [8], where we propose that a triangle singularity mechanism

---

\* zhaog@ihep.ac.cn

† zoubs@ihep.ac.cn

(TSM) via the intermediate  $K^*\bar{K} + c.c.$  rescatterings would lead to significant enhancement of the isospin violating decay, i.e.  $\eta(1405/1475) \rightarrow K^*\bar{K} + c.c. \rightarrow f_0(980)\pi$ . In this transition, the dominant contributions would come from such a specific kinematic region that all the intermediate mesons in the triangle loop are literally on-shell. The identification of such a mechanism seems to be nontrivial since it can naturally explain the narrow width of the  $f_0(980)$  observed in the two pion invariant mass spectrum. Consequently, it raises an essential issue concerning the nature of  $\eta(1405/1475)$  since the TSM can also contribute to the decays of  $\eta(1405/1475) \rightarrow K\bar{K}\pi$  and  $\eta\pi\pi$ , and distort the lineshapes and shift the peak positions of the  $\eta(1405/1475)$  in those decay channels. As a result, a coherent study of  $\eta(1405/1475) \rightarrow K\bar{K}\pi$ ,  $\eta\pi\pi$ , and  $3\pi$  is necessary and could be a key towards a better understanding of the  $\eta(1405/1475)$  puzzle.

In this work, we shall provide a detailed analysis of  $\eta(1405/1475) \rightarrow K\bar{K}\pi$ ,  $\eta\pi\pi$ , and  $3\pi$ . We shall show that only one  $0^{-+}$  isoscalar state, namely  $\eta(1440)$ , is needed in this mass region. With this ‘‘one state’’ assumption, we shall demonstrate that the TSM can lead to different mass spectra for  $\eta(1440) \rightarrow K\bar{K}^* + c.c.$ ,  $a_0(980)\pi^0$ , and  $f_0(980)\pi$ . In  $J/\psi \rightarrow \gamma\eta(1440)$ , with  $\eta(1440) \rightarrow K\bar{K}^* + c.c.$ ,  $a_0(980)\pi^0$ , and  $f_0(980)\pi$ , another possible contribution to the same final states is via  $f_1(1420)$ . Since the mass of  $f_1(1420)$  is similar to that of  $\eta(1440)$ , we should investigate the role played by  $f_1(1420)$  in these processes. In particular, due to the similar masses between  $f_1(1420)$  and  $\eta(1440)$ , the decay of  $f_1(1420)$  would also experience the TSM. Therefore, a helicity analysis of the invariant mass spectrum for the overlapping  $f_1(1420)$  and  $\eta(1440)$  is necessary. In comparison with the results reported in Ref. [8], we have detailed all the analysis by including the  $f_1(1420)$  contributions. We confirm the BESIII results by detailed helicity analysis from which we can extract the invariant mass spectra for  $\eta(1440)$  in different channels. These features as a consequence of the TSM could be a natural solution for the long-standing puzzle about the nature of  $\eta(1405/1475)$  in experimental analyses.

We also mention that the  $\eta(1405/1475) \rightarrow 3\pi$  decay was also studied in Ref. [9] recently in a chiral unitary approach. By exhausting several models and taking constraints from the meson-meson scatterings, the authors confirm that only  $a_0(980)$ - $f_0(980)$  mixing can not explain the BES result [6] and the inclusion of the triangular diagrams is necessary [8].

The rest part of this paper is organized as follows: the formalism is presented in Sec. II. Section III is devoted to the numerical results and discussions. Our conclusion is given in Sec. IV.

## II. FORMALISM

### A. Effective Lagrangians and transition amplitudes

The effective Lagrangians for the  $\eta(1440)$  production have been presented in Ref. [8]. Here, we include the  $f_1(1420)$  contribution and list the effective Lagrangians as the following:

$$\mathcal{L}_{V_1V_2P} = g_{V_1V_2P}\varepsilon_{\mu\nu\rho\sigma}p_{V_1}^\mu p_{V_2}^\nu \psi_{V_1}^\rho \psi_{V_2}^\sigma \psi_P, \quad (1)$$

$$\mathcal{L}_{VP_1P_2} = g_{VP_1P_2}(\psi_{P_1}\partial_\mu\psi_{P_2} - \psi_{P_2}\partial_\mu\psi_{P_1})\psi_V^\mu, \quad (2)$$

$$\mathcal{L}_{SP_1P_2} = g_{SP_1P_2}\psi_S\psi_{P_1}\psi_{P_2}, \quad (3)$$

$$\mathcal{L}_{AVP} = g_{AVP}\psi_A^\mu\psi_{V\mu}\psi_P, \quad (4)$$

$$\mathcal{L}_{\psi\gamma f_1} = g_1\varepsilon_{\mu\nu\rho\sigma}\partial^\mu\psi_\psi^\nu\psi_\gamma^\rho\psi_{f_1}^\sigma + g_2\varepsilon_{\mu\nu\rho\sigma}\partial^\mu\psi_\psi^\lambda\partial^\lambda\partial^\nu\psi_\gamma^\rho\psi_{f_1}^\sigma, \quad (5)$$

where  $S$ ,  $P$ ,  $V$  and  $A$  stand for four types of fields: scalar, pseudoscalar, vector and axialvector, respectively. For  $\eta(1440)$  the same diagrams as in Ref. [8] are calculated, while for  $f_1(1420)$  the similar diagrams are listed in Fig. 1. Figure 1(1a)-(1b) are for  $f_1(1420) \rightarrow K\bar{K}\pi$  through  $K^*\bar{K}$  and  $a_0(980)\pi$  channels. Figure 1(2a)-(2b) are for  $f_1(1420) \rightarrow \pi^+\pi^-\pi^0$  through the TSM and  $a_0 - f_0$  mixing. Figure 1(3) is for  $f_1(1420) \rightarrow \eta\pi^0\pi^0$ , where we assume that  $a_0^0(980)\pi^0$  gives the main contribution.

Our kinematics conventions are shown in Fig. 2. Some common functions are defined as follows:

$$G_f = \frac{1}{s - m_f^2 + i\sqrt{s}\Gamma_f(s)}, \quad (6)$$

$$G_a = \frac{1}{s - m_a^2 + i\sqrt{s}\Gamma_a(s)}, \quad (7)$$

$$\Gamma_a(s) = \frac{g_{aK\bar{K}}^2(\rho(\sqrt{s}, m_{K^0}, m_{\bar{K}^0}) + \rho(\sqrt{s}, m_{K^+}, m_{K^-}))}{16\pi\sqrt{s}} + \frac{g_{a\pi\eta}^2\rho(\sqrt{s}, m_{\pi^0}, m_\eta)}{16\pi\sqrt{s}}, \quad (8)$$

$$\Gamma_f(s) = \frac{g_{fK\bar{K}}^2(\rho(\sqrt{s}, m_{K^0}, m_{\bar{K}^0}) + \rho(\sqrt{s}, m_{K^+}, m_{K^-}))}{16\pi\sqrt{s}}$$

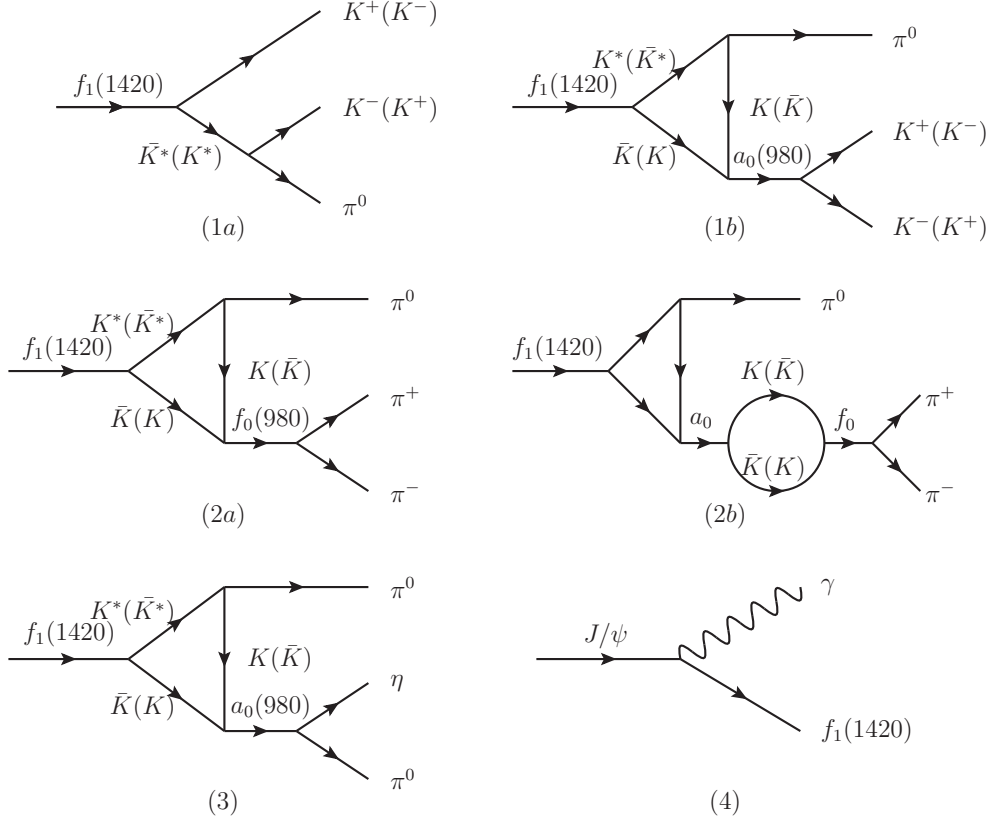


FIG. 1: Feynman diagrams for the  $f_1(1420)$  decays and its production in  $J/\psi$  radiative decay. Similar diagrams for  $\eta(1440)$  have been given in Ref. [8].

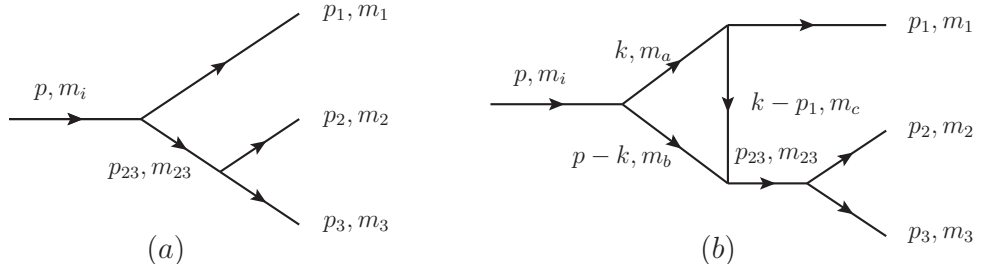


FIG. 2: Kinematics defined in our formalism.

$$+ \frac{g_{f\pi\pi}^2 (\rho(\sqrt{s}, m_{\pi^0}, m_{\pi^0}) + 2\rho(\sqrt{s}, m_{\pi^+}, m_{\pi^-}))}{16\pi\sqrt{s}}, \quad (9)$$

$$\rho(\sqrt{s}, m_A, m_B) = \frac{1}{s} \sqrt{(s - (m_A + m_B)^2)(s - (m_A - m_B)^2)}. \quad (10)$$

Then, the typical loop integrals can be expressed as

$$\hat{I}_{\eta 1} = i \int \frac{d^4 k}{(2\pi)^4} (2p-k)^\mu (2p_1-k)^\nu \frac{(-g_{\mu\nu} + \frac{k_\mu k_\nu}{m_a^2})}{k^2 - m_a^2} \frac{1}{(p-k)^2 - m_b^2} \frac{1}{(k-p_1)^2 - m_c^2}, \quad (11)$$

$$\begin{aligned} \hat{I}_{f1} &= i \int \frac{d^4 k}{(2\pi)^4} \epsilon_p^\mu (2p_1-k)^\nu \frac{(-g_{\mu\nu} + \frac{k_\mu k_\nu}{m_a^2})}{k^2 - m_a^2} \frac{1}{(p-k)^2 - m_b^2} \frac{1}{(k-p_1)^2 - m_c^2} \\ &= \epsilon_p^\mu (c_p p_\mu + c_{p_1} p_{1\mu}), \end{aligned} \quad (12)$$

$$\hat{I}_{f1b} = \hat{I}_{f1}(1 \leftrightarrow 2) = \epsilon_p^\mu (d_p p_\mu + d_{p_2} p_{2\mu}). \quad (13)$$

Taking into account that the relative signs between the charged and neutral loops are positive in isospin-conserving processes but negative in isospin-violating processes, it is convenient to define

$$c_p^+ \equiv c_p^c g_{k^* K \pi}^c + c_p^n g_{k^* K \pi}^n, \quad (14)$$

$$c_p^- \equiv c_p^c g_{k^* K \pi}^c - c_p^n g_{k^* K \pi}^n, \quad (15)$$

$$c_{p_1}^+ \equiv c_{p_1}^c g_{k^* K \pi}^c + c_{p_1}^n g_{k^* K \pi}^n, \quad (16)$$

$$c_{p_1}^- \equiv c_{p_1}^c g_{k^* K \pi}^c - c_{p_1}^n g_{k^* K \pi}^n, \quad (17)$$

where the superscripts ‘c’ and ‘n’ denote the charged and neutral loops, respectively. We also define  $\hat{I}_{\eta 1}^\pm$ ,  $d_p^\pm$  and  $d_{p_2}^\pm$  for  $\hat{I}_{f1b}$  in a similar way.

The invariant amplitudes in Fig. 1 can then be expressed as

$$\begin{aligned} \mathcal{M}_{1a} &= g_{f_1 K^* K} g_{K^* K \pi} \left[ \epsilon_p^\mu \frac{(-g_{\mu\nu} + p_{23\mu} p_{23\nu})}{s_{23} - m_V^2 + i m_V \Gamma_V} (p_3 - p_2)^\nu + (2 \leftrightarrow 1) \right] \\ &= g_{f_1 K^* K} g_{K^* K \pi} \times \epsilon_p^\mu (c_1 p_{1\mu} + c_2 p_{2\mu} + c_3 p_{3\mu}), \end{aligned} \quad (18)$$

$$\overline{\sum_{spin}} |\mathcal{M}_{1a}|^2 = \frac{1}{3} g_{f_1 K^* K}^2 g_{K^* K \pi}^2 \left( -g^{\mu\nu} + \frac{p^\mu p^\nu}{m_{f_1}^2} \right) (c_1 p_{1\mu} + c_2 p_{2\mu} + c_3 p_{3\mu}) (c_1^* p_{1\nu} + c_2^* p_{2\nu} + c_3^* p_{3\nu}), \quad (19)$$

$$\begin{aligned} \mathcal{M}_{1b} &= 2g_{f_1 K^* K} g_{aK\bar{K}}^2 G_a(s_{23}) \left( g_{K^* K \pi}^c \hat{I}_{f1}^c + g_{K^* K \pi}^n \hat{I}_{f1}^n \right) \\ &= 2g_{f_1 K^* K} g_{aK\bar{K}}^2 G_a(s_{23}) \times \epsilon_p^\mu (p_\mu c_p^+ + p_{1\mu} c_{p_1}^+), \end{aligned} \quad (20)$$

$$\overline{\sum_{spin}} |\mathcal{M}_{1b}|^2 = \frac{4}{3} g_{f_1 K^* K}^2 g_{aK\bar{K}}^4 |G_a(s_{23})|^2 \left( -g^{\mu\nu} + \frac{p^\mu p^\nu}{m_{f_1}^2} \right) (p_\mu c_p^+ + p_{1\mu} c_{p_1}^+) (p_\nu c_p^{+*} + p_{1\nu} c_{p_1}^{+*}), \quad (21)$$

$$\begin{aligned} \mathcal{M}_{2a} &= 2\sqrt{2} g_{f_1 K^* K} g_{fK\bar{K}} g_{f\pi\pi} G_f(s_{23}) \left( g_{K^* K \pi}^c \hat{I}_{f1}^c - g_{K^* K \pi}^n \hat{I}_{f1}^n \right) \\ &= 2\sqrt{2} g_{f_1 K^* K} g_{fK\bar{K}} g_{f\pi\pi} G_f(s_{23}) \times \epsilon_p^\mu (p_\mu c_p^- + p_{1\mu} c_{p_1}^-), \end{aligned} \quad (22)$$

$$\overline{\sum_{spin}} |\mathcal{M}_{2a}|^2 = \frac{8}{3} g_{f_1 K^* K}^2 g_{fK\bar{K}}^2 g_{f\pi\pi}^2 |G_f(s_{23})|^2 \left( -g^{\mu\nu} + \frac{p^\mu p^\nu}{m_{f_1}^2} \right) (p_\mu c_p^- + p_{1\mu} c_{p_1}^-) (p_\nu c_p^{-*} + p_{1\nu} c_{p_1}^{-*}), \quad (23)$$

$$\mathcal{M}_{2b} = \mathcal{M}_{1b} \times \sqrt{2} g_{fK\bar{K}} g_{f\pi\pi} G_f(s_{23}) (loop2^c - loop2^n), \quad (24)$$

$$\overline{\sum_{spin}} |\mathcal{M}_{2b}|^2 = \left( \overline{\sum_{spin}} |\mathcal{M}_{1b}|^2 \right) \times 2g_{fK\bar{K}}^2 g_{f\pi\pi}^2 |G_f(s_{23})|^2 |loop2^c - loop2^n|^2, \quad (25)$$

$$\begin{aligned} \mathcal{M}_3 &= 2g_{f_1 K^* K} g_{aK\bar{K}} g_{a\pi\eta} \left[ G_a(s_{23}) \left( g_{K^* K \pi}^c \hat{I}_{f1}^c + g_{K^* K \pi}^n \hat{I}_{f1}^n \right) + (2 \leftrightarrow 1) \right] \\ &= 2g_{f_1 K^* K} g_{aK\bar{K}} g_{a\pi\eta} \times \epsilon_p^\mu \left[ G_a(s_{23}) (p_\mu c_p^+ + p_{1\mu} c_{p_1}^+) + (2 \leftrightarrow 1) \right], \end{aligned} \quad (26)$$

$$\begin{aligned} \overline{\sum_{spin}} |\mathcal{M}_3|^2 &= \frac{2}{3} g_{f_1 K^* K}^2 g_{aK\bar{K}}^2 g_{a\pi\eta}^2 \left( -g^{\mu\nu} + \frac{p^\mu p^\nu}{m_{f_1}^2} \right) \left[ |G_a(s_{23})|^2 (p_\mu c_p^+ + p_{1\mu} c_{p_1}^+) (p_\nu c_p^{+*} + p_{1\nu} c_{p_1}^{+*}) \right. \\ &\quad + |G_a(s_{13})|^2 (p_\mu d_p^+ + p_{2\mu} d_{p_2}^+) (p_\nu d_p^{+*} + p_{2\nu} d_{p_2}^{+*}) \\ &\quad + G_a(s_{23}) G_a(s_{13})^* (p_\mu c_p^+ + p_{1\mu} c_{p_1}^+) (p_\nu d_p^{+*} + p_{2\nu} d_{p_2}^{+*}) \\ &\quad \left. + G_a(s_{23})^* G_a(s_{13}) (p_\mu c_p^{+*} + p_{1\mu} c_{p_1}^{+*}) (p_\nu d_p^+ + p_{2\nu} d_{p_2}^+) \right], \end{aligned} \quad (27)$$

$$\mathcal{M}_4 = g_1 \epsilon_{\mu\nu\rho\sigma} p_\psi^\mu \epsilon_\psi^\nu \epsilon_{f_1}^\rho \epsilon_{f_1}^\sigma + g_2 \epsilon_{\mu\nu\rho\sigma} p_\psi^\mu p_{f_1}^\nu \epsilon_\psi^\rho \epsilon_{f_1}^\sigma \epsilon_\psi \cdot p_{f_1} B_2(Q) . \quad (28)$$

In Eq. (27), we have put the identical factor 1/2 in the squared amplitude. The parametrization of Eq. (28) is taken from Ref. [10] and  $B_2(Q)$  is the Blatt-Weisskopf barrier factor

$$B_2(Q) = \sqrt{\frac{1}{Q^4 + 3Q^2 Q_0^2 + 9Q_0^4}} , \quad (29)$$

where  $Q$  is the decay momentum, and  $Q_0$  is a hadron scale parameter  $Q_0 = 0.197321/R$  GeV with  $R$  the radius of the centrifugal barrier in fermi. In this paper we adopt  $R = 0.35$  fm which is about the radius of  $J/\psi$ .

### 1. Helicity amplitudes

In experiment, the quantum number of an intermediate state  $X$  is generally determined by measuring the angular distribution of the  $X$  decays. To proceed, we first make a model-independent analysis of the helicity structure of the transition matrix element which would allow us to separate different partial waves. Then, by comparing with the angular distributions measured by experiment, we can extract the dynamic coupling strengths for different partial waves.

For a decay process  $a \rightarrow b + c$  with spin, helicity and parity  $(s_i, \lambda_i, \eta_i)_{i=a,b,c}$ , the decay amplitude in the rest frame of  $a$  can be expressed as [11],

$$\mathcal{M}_{\lambda_b \lambda_c}^{s_a}(\theta, \phi; \lambda_a) \propto D_{\lambda_a, \lambda_b - \lambda_c}^{s_a*}(\phi, \theta, 0) F_{\lambda_b \lambda_c}^{s_a} , \quad (30)$$

where  $D_{\lambda_a, \lambda_b - \lambda_c}^{s_a*}(\phi, \theta, 0)$  is the rotation function, and  $F_{\lambda_b \lambda_c}^{s_a}$  is the helicity-coupling amplitude which is independent of angular variables. It satisfies two constraints taking into account angular momentum conservation and Parity conservation:

$$|\lambda_b - \lambda_c| \leq s_a , \quad (31)$$

$$F_{\lambda_b \lambda_c}^{s_a} = \eta_a \eta_b \eta_c (-)^{s_a - s_b - s_c} F_{-\lambda_b - \lambda_c}^{s_a} . \quad (32)$$

From these relations, we can find out the independent helicity-coupling amplitudes.

As follows, we will re-analyze the angular distributions of the recoiled photon in  $J/\psi \rightarrow \gamma X$  and the recoiled  $f_0(980)$  in  $X \rightarrow f_0(980)\pi$  decays which are measured by the BESIII experiment [6]. Now as a preparation, we derive the helicity amplitudes of each vertex from the Lagrangians in Eqs. (1)-(5).

In  $J/\psi \rightarrow \gamma f_1$ , the helicity amplitude with transversely polarized  $f_1$  can be expressed as

$$\begin{aligned} \langle \lambda_\gamma, \lambda_{f_1} = \pm 1 | \hat{S} | \lambda_\psi \rangle &= g_1 \epsilon_{\mu\nu\rho\sigma} p_\psi^\mu \epsilon_\psi^\nu \epsilon_{f_1}^{*\rho} \epsilon_{f_1}^{*\sigma} + g_2 B_2(Q) \epsilon_{\mu\nu\rho\sigma} p_\psi^\mu p_{f_1}^\nu \epsilon_\psi^\rho \epsilon_{f_1}^{*\sigma} \epsilon_\psi \cdot p_{f_1} \\ &= -ig_1 \lambda_\gamma m_\psi D_{\lambda_\psi 0}^{1*}(\phi, \theta, 0) + ig_2 B_2(Q) \lambda_\gamma m_\psi Q^2 D_{\lambda_\psi 0}^{1*}(\phi, \theta, 0) \\ &= D_{\lambda_\psi 0}^{1*}(\phi, \theta, 0) F_{\lambda_\gamma \lambda_{f_1}}^1 , \end{aligned} \quad (33)$$

which is nonvanishing with  $\lambda_\gamma = \lambda_{f_1}$ , and

$$F_{\lambda_\gamma \lambda_{f_1}}^1 = -ig_1 \lambda_\gamma m_\psi + ig_2 \lambda_\gamma m_\psi Q^2 B_2(Q) . \quad (34)$$

So the independent amplitude is

$$F_{11}^{1a} = im_\psi [-g_1 + g_2 Q^2 B_2(Q)] . \quad (35)$$

When  $f_1$  is longitudinally polarized, the  $g_2$  term will have no contribution. The helicity amplitude is

$$\begin{aligned} \langle \lambda_\gamma, \lambda_{f_1} = 0 | \hat{S} | \lambda_\psi \rangle &= g_1 \epsilon_{\mu\nu\rho\sigma} p_\psi^\mu \epsilon_\psi^\nu \epsilon_{f_1}^{*\rho} \epsilon_{f_1}^{*\sigma} \\ &= -ig_1 \lambda_\gamma m_\psi \frac{E_{f_1}}{m_{f_1}} D_{\lambda_\psi \lambda_\gamma}^{1*}(\phi, \theta, 0) \\ &= D_{\lambda_\psi \lambda_\gamma}^{1*}(\phi, \theta, 0) F_{\lambda_\gamma 0}^1 , \end{aligned} \quad (36)$$

with

$$F_{\lambda_\gamma 0}^1 = -ig_1 \lambda_\gamma m_\psi \frac{E_{f_1}}{m_{f_1}} . \quad (37)$$

So the independent amplitude is

$$F_{10}^{1a} = -ig_1 m_\psi \frac{E_{f_1}}{m_{f_1}}. \quad (38)$$

For  $f_1 \rightarrow f_0(980)\pi^0$ , the helicity amplitude can be written as

$$\begin{aligned} \langle f_0\pi|\hat{S}|f_1\rangle &= 2g_{f_1K^*K}g_{f_0KK} \left[ g_{K^*K\pi}^c \hat{I}_{f_1}^c - g_{K^*K\pi}^n \hat{I}_{f_1}^n \right] \\ &= 2g_{f_1K^*K}g_{f_0KK} \epsilon_p^\mu (p_\mu c_p^- + p_{1\mu} c_{p_1}^-) \\ &= 2g_{f_1K^*K}g_{f_0KK} c_{p_1}^- \epsilon_p \cdot p_1 \\ &= D_{\lambda_{f_1}0}^{1*}(\phi, \theta, 0) F_{00}^{1b}, \end{aligned} \quad (39)$$

where we have used the relation  $\epsilon_p \cdot p = 0$ . Also, in the helicity frame of  $f_1(1420)$ , we have

$$\epsilon_p \cdot p_1 = -D_{\lambda_{f_1}0}^{1*}(\phi, \theta, 0) Q. \quad (40)$$

So the independent amplitude is

$$F_{00}^{1b} = -2g_{f_1K^*K}g_{f_0KK} c_{p_1}^- Q. \quad (41)$$

Similarly, the helicity amplitude for  $J/\psi \rightarrow \gamma\eta(1440)$  can be obtained with both  $J/\psi$  and  $\gamma$  transversely polarized:

$$\begin{aligned} \langle \lambda_\gamma\eta(1440)|\hat{S}|\lambda_\psi\rangle &= g_{\psi\gamma\eta_1} \epsilon_{\mu\nu\rho\sigma} p_\psi^\mu q_\gamma^\nu \epsilon_\psi^\rho \epsilon_\gamma^\sigma \\ &= -i\lambda_\gamma g_{\psi\gamma\eta_1} m_\psi |\vec{q}| D_{\lambda_\psi\lambda_\gamma}^{1*}(\phi, \theta, 0) \\ &= D_{\lambda_\psi\lambda_\gamma}^{1*}(\phi, \theta, 0) F_{\lambda_\gamma 0}^{1c}, \end{aligned} \quad (42)$$

with

$$F_{\lambda_\gamma 0}^{1c} = -i\lambda_\gamma g_{\psi\gamma\eta_1} m_\psi |\vec{q}|. \quad (43)$$

For  $\eta(1440) \rightarrow f_0(980)\pi^0$ , the helicity amplitude is

$$\begin{aligned} \langle f_0\pi|\hat{S}|\eta(1440)\rangle &= 2g_{\eta_1K^*K}g_{f_0KK} (g_{K^*K\pi}^c \hat{I}_{f_1}^c - g_{K^*K\pi}^n \hat{I}_{f_1}^n) \\ &= F_{00}^{0d}. \end{aligned} \quad (44)$$

## B. Angular distribution

By combining the two-body decay amplitudes in the helicity frame, we can derive the total helicity amplitudes for the chain process  $J/\psi \rightarrow \gamma X \rightarrow \gamma f_0(980)\pi^0$  as shown in Fig. 3 and extract the angular distributions to compare with the experimental data [6].

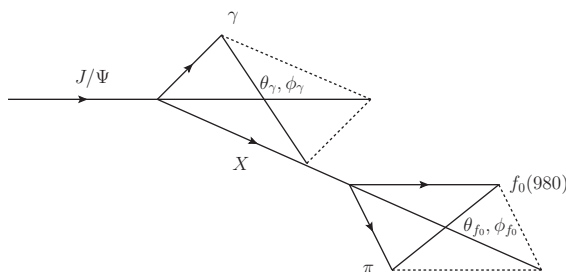


FIG. 3: The kinematics for the chain process  $J/\psi \rightarrow \gamma X \rightarrow \gamma f_0(980)\pi^0$ .

For  $X$  being  $\eta(1440)$ , the total helicity amplitude can be expressed as

$$A_{\eta_1}(\lambda_\psi, \lambda_\gamma) \propto D_{\lambda_\psi \lambda_\gamma}^{1*}(\phi_\gamma, \theta_\gamma, 0) F_{\lambda_\gamma 0}^{1c} \frac{1}{s - m_{\eta_1}^2 + im_{\eta_1} \Gamma_{\eta_1}} F_{00}^{0d}. \quad (45)$$

The angular distribution is

$$\begin{aligned} \frac{d\sigma_{\eta_1}}{d\Omega} &\propto \sum_{\lambda_\psi, \lambda_\gamma = \pm 1} |A_{\eta_1}(\lambda_\psi, \lambda_\gamma)|^2 \\ &\propto \sum_{\lambda_\psi, \lambda_\gamma = \pm 1} \left| D_{\lambda_\psi \lambda_\gamma}^{1*}(\phi_\gamma, \theta_\gamma, 0) \right|^2 \\ &= 1 + \cos^2 \theta_\gamma, \end{aligned} \quad (46)$$

where  $d\Omega \equiv d\Omega_\gamma d\Omega_{f_0}$  with  $d\Omega_\gamma \equiv d \cos \theta_\gamma d\phi_\gamma$  and  $d\Omega_{f_0} \equiv d \cos \theta_{f_0} d\phi_{f_0}$ . One step further, we obtain

$$\frac{d\sigma_{\eta_1}}{d \cos \theta_\gamma} \propto 1 + \cos^2 \theta_\gamma, \quad (47)$$

$$\frac{d\sigma_{\eta_1}}{d \cos \theta_{f_0}} \propto \text{const}, \quad (48)$$

for the angular distributions of  $\theta_\gamma$  and  $\theta_{f_0(980)}$ , respectively. These expressions are the same as those adopted in Ref. [6].

For  $X$  being  $f_1(1420)$ , the total helicity amplitude of the chain process can be expressed as

$$A_{f_1}(\lambda_\psi, \lambda_\gamma, \lambda_{f_1}) \propto D_{\lambda_\psi, \lambda_\gamma - \lambda_{f_1}}^{1*}(\phi_\gamma, \theta_\gamma, 0) F_{\lambda_\gamma \lambda_{f_1}}^{1a} \frac{1}{s - m_{f_1}^2 + im_{f_1} \Gamma_{f_1}} D_{\lambda_{f_1} 0}^{1*}(\phi_{f_0}, \theta_{f_0}, 0) F_{00}^{1b}. \quad (49)$$

The angular distribution via  $f_1(1420)$  is

$$\begin{aligned} \frac{d\sigma_{f_1}}{d\Omega} &\propto \sum_{\lambda_\psi, \lambda_\gamma = \pm 1} \left| \sum_{\lambda_{f_1} = 0, \pm 1} A_{f_1}(\lambda_\psi, \lambda_\gamma, \lambda_{f_1}) \right|^2 \\ &\propto \sum_{\lambda_\psi, \lambda_\gamma = \pm 1} \left| \alpha D_{\lambda_\psi 0}^{1*}(\phi_\gamma, \theta_\gamma, 0) D_{\lambda_\gamma 0}^{1*}(\phi_{f_0}, \theta_{f_0}, 0) + D_{\lambda_\psi, \lambda_\gamma}^{1*}(\phi_\gamma, \theta_\gamma, 0) D_{00}^{1*}(\phi_{f_0}, \theta_{f_0}, 0) \right|^2 \\ &= \alpha_1^2 \sin^2 \theta_{f_0} \sin^2 \theta_\gamma + \frac{\alpha_1}{2} \cos \phi_\alpha \cos \phi_{f_0} \sin 2\theta_{f_0} \sin 2\theta_\gamma + \cos^2 \theta_{f_0} (\cos^2 \theta_\gamma + 1), \end{aligned} \quad (50)$$

where  $\alpha \equiv \alpha_1 e^{i\phi_\alpha}$  is the ratio of the  $\lambda_{f_1} = \pm 1$  amplitude to that of  $\lambda_{f_1} = 0$ . By integrating over corresponding polar angles in the above double distribution, one has access to the angular distributions of  $\theta_\gamma$  and  $\theta_{f_0}$ , respectively, for the intermediate  $f_1(1420)$ :

$$\frac{d\sigma_{f_1}}{d \cos \theta_\gamma} \propto 1 + 2\alpha_1^2 + (1 - 2\alpha_1^2) \cos^2 \theta_\gamma, \quad (51)$$

$$\frac{d\sigma_{f_1}}{d \cos \theta_{f_0}} \propto 2 + (\alpha_1^2 - 2) \sin^2 \theta_{f_0}. \quad (52)$$

With both  $\eta(1440)$  and  $f_1(1420)$  contributing to the chain process, the total helicity amplitude can be obtained in a similar way, namely,

$$\begin{aligned} A_{\eta_1 + f_1}(\lambda_\psi, \lambda_\gamma) &= D_{\lambda_\psi \lambda_\gamma}^{1*}(\phi_\gamma, \theta_\gamma, 0) F_{\lambda_\gamma 0}^{1c} \frac{1}{s - m_{\eta_1}^2 + im_{\eta_1} \Gamma_{\eta_1}} F_{00}^{0d} \\ &\quad + D_{\lambda_\psi 0}^{1*}(\phi_\gamma, \theta_\gamma, 0) D_{\lambda_\gamma 0}^{1*}(\phi_{f_0}, \theta_{f_0}, 0) F_{\lambda_\gamma \lambda_\gamma}^{1a} \frac{1}{s - m_{f_1}^2 + im_{f_1} \Gamma_{f_1}} F_{00}^{1b} \\ &\quad + D_{\lambda_\psi \lambda_\gamma}^{1*}(\phi_\gamma, \theta_\gamma, 0) D_{00}^{1*}(\phi_{f_0}, \theta_{f_0}, 0) F_{\lambda_\gamma 0}^{1a} \frac{1}{s - m_{f_1}^2 + im_{f_1} \Gamma_{f_1}} F_{00}^{1b} \\ &\propto \lambda_\gamma \left[ r D_{\lambda_\psi \lambda_\gamma}^{1*}(\phi_\gamma, \theta_\gamma, 0) + \alpha D_{\lambda_\psi 0}^{1*}(\phi_\gamma, \theta_\gamma, 0) D_{\lambda_\gamma 0}^{1*}(\phi_{f_0}, \theta_{f_0}, 0) + D_{\lambda_\psi \lambda_\gamma}^{1*}(\phi_\gamma, \theta_\gamma, 0) D_{00}^{1*}(\phi_{f_0}, \theta_{f_0}, 0) \right] \end{aligned} \quad (53)$$

where we have applied the selection rule  $\lambda_{f_1} = \lambda_\gamma$  for the transversely polarized  $f_1(1420)$ ;  $r \equiv r_1 e^{i\phi_r}$  is the ratio of the  $\eta(1440)$  amplitude to that of  $f_1(1420)$  with  $\lambda_{f_1} = 0$ . Then the angular distribution becomes

$$\begin{aligned} \frac{d\sigma_{\eta_1+f_1}}{d\Omega} &\propto \sum_{\lambda_\psi, \lambda_\gamma=\pm 1} |A_{\eta_1+f_1}(\lambda_\psi, \lambda_\gamma)|^2 \\ &= r_1^2 (\cos 2\theta_\gamma + 3) + 2r_1 \alpha_1 \sin \theta_{f_0} \sin 2\theta_\gamma \cos \phi_{f_0} \cos(\phi_\alpha - \phi_r) + 2r_1 \cos \theta_{f_0} \cos \phi_r (\cos 2\theta_r + 3) \\ &\quad + 2\alpha_1^2 \sin^2 \theta_{f_0} \sin^2 \theta_\gamma + \alpha_1 \cos \phi_\alpha \sin 2\theta_{f_0} \sin 2\theta_\gamma \cos \phi_{f_0} + \cos^2 \theta_{f_0} (\cos 2\theta_\gamma + 3). \end{aligned} \quad (54)$$

It is easy to show that Eqs. (46) and (50) can be reproduced by setting the corresponding resonance couplings to vanish. Similarly, the angular distributions of  $\theta_\gamma$  and  $\theta_{f_0}$  can be obtained

$$\frac{d\sigma_{\eta_1+f_1}}{d \cos \theta_\gamma} \propto 1 + 2\alpha_1^2 + 3r_1^2 + (1 - 2\alpha_1^2 + 3r_1^2) \cos^2 \theta_\gamma, \quad (55)$$

$$\frac{d\sigma_{\eta_1+f_1}}{d \cos \theta_{f_0}} \propto \alpha_1^2 + 2r_1^2 + 4r_1 \cos \phi_r \cos \theta_{f_0} + (2 - \alpha_1^2) \cos^2 \theta_{f_0}. \quad (56)$$

Checking Eqs. (47), (51) and (55), one can see that the  $\cos \theta_\gamma$  distribution is always symmetric as a feature of a two-body decay. In contrast, the angular distribution of  $\cos \theta_{f_0}$  turns out to be nontrivial. As shown by Eqs. (48), (52) and (56), the contributions from different states with different quantum numbers are encoded in the angular distribution of  $\cos \theta_{f_0}$ . By fitting the experimental data, the coupling parameters can thus be determined which alternatively would provide information about the contributing resonances. As shown by Fig. 3 of Ref. [6], the  $\cos \theta_{f_0}$  distribution is apparently asymmetric which indicates some contributions from the  $f_1(1420)$  production besides  $\eta(1440)$ .

With the explicit total helicity amplitude in Eq. (53), we can express the differential width as

$$d\Gamma = \frac{1}{(2\pi)^5} \frac{1}{16m_\psi^2} |A_{\eta_1+f_1}|^2 |\vec{p}_\gamma| |\vec{p}_{f_0}| d\sqrt{s_X} d\Omega_\gamma d\Omega_{f_0}. \quad (57)$$

We can define the following quantities by integrating the invariant mass  $\sqrt{s_X}$  of the  $f_0(980)\pi^0$ :

$$A_1 = \int d\sqrt{s_X} |\vec{p}_\gamma| |\vec{p}_{f_0}| \left| \frac{F_{10}^{1c} F_{00}^{0d}}{s_X - m_{\eta_1}^2 + im_{\eta_1} \Gamma_{\eta_1}} \right|^2, \quad (58)$$

$$A_2 = \int d\sqrt{s_X} |\vec{p}_\gamma| |\vec{p}_{f_0}| \left| \frac{F_{11}^{1a} F_{00}^{1b}}{s_X - m_{f_1}^2 + im_{f_1} \Gamma_{f_1}} \right|^2, \quad (59)$$

$$A_3 = \int d\sqrt{s_X} |\vec{p}_\gamma| |\vec{p}_{f_0}| \left| \frac{F_{10}^{1a} F_{00}^{1b}}{s_X - m_{f_1}^2 + im_{f_1} \Gamma_{f_1}} \right|^2, \quad (60)$$

which can thus be related to the quantities measured in experiment, i.e.

$$\alpha_1^2 = \frac{A_2}{A_3}, \quad r_1^2 = \frac{A_1}{A_3}. \quad (61)$$

From these relations, we can extract the information about the couplings from the angular distribution analysis.

To compare with the experimental measurement of the unpolarized partial decay width in terms of the recoiled energy  $s$  by the photon in  $J/\psi \rightarrow \gamma X \rightarrow \gamma ABC$ , the following standard expression is adopted,

$$\frac{d\Gamma_{J/\psi \rightarrow \gamma X \rightarrow \gamma ABC}}{d\sqrt{s}} = \frac{2s \Gamma_{J/\psi \rightarrow \gamma X}(s) \times \Gamma_{X \rightarrow ABC}(s)}{\pi (s - m_X^2)^2 + \Gamma_X^2 m_X^2}, \quad (62)$$

where  $s$  is the four-momentum square of  $X = \eta(1440)/f_1(1420)$  in the reaction. A constant width  $\Gamma(f_1(1420)) = 0.0549$  GeV is adopted for  $f_1(1420)$  [4], while for  $\eta(1440)$ , both constant width and energy-dependent form are adopted,

$$\Gamma_{\eta(1440)}(s) = \Gamma_{\eta(1440) \rightarrow K^* K \rightarrow K \bar{K} \pi}(s) = \Gamma_{1a}(s), \quad (63)$$

where  $\Gamma_{1a}$  corresponds to Fig. 1(1a).



### III. RESULTS AND DISCUSSIONS

In this part, we present our analyses and numerical results. First we demonstrate explicitly that the TSM is dominant in  $\eta(1440) \rightarrow 3\pi$ , and the main contribution is indeed from such a kinematic region that all the internal particles are close to their mass shells. Then, we give the fitting results about  $\eta(1440)$  from  $K\bar{K}\pi$  spectrum and show the predictions of  $\pi^+\pi^-\pi^0$  and  $\eta\pi^0\pi^0$  which are consistent with Ref. [8]. By including  $f_1(1420)$ , we extract the couplings of  $f_1(1420)$  through the analysis of the angular distribution of  $\pi^+\pi^-\pi^0$  channel [6]. Finally, we show that the combined results for both  $\eta(1440)$  and  $f_1(1420)$  in comparison with the BES data would allow us to draw a conclusion on the anomalously large isospin violations observed in  $\eta(1405) \rightarrow 3\pi$  and the nature of  $\eta(1405)$  and  $\eta(1475)$ .

#### A. Loop integral

Here we discuss in detail the calculation of  $\hat{I}_{\eta_1}$  and  $\hat{I}_{f_1}$  in Eqs. (11)-(12). What we actually need in  $\hat{I}_{f_1}$  is the coefficients  $c_p$  and  $c_{p1}$ . We use two methods to calculate the loops:

1. We directly calculate  $\hat{I}_{\eta_1}$  and  $\hat{I}_{f_1}$  by *LoopTools* without any form factors. The UV divergences are regularized dimensionally by  $\Delta = 2/(4-D) - \gamma_E + \log 4\pi$ , where  $\Delta$  can be adjusted and the default value is  $\Delta = 0$ .
2. The exponential form factor method as applied in Ref. [12]. Namely, an exponential form factor as follows is included in  $\hat{I}_{\eta_1}$  and  $\hat{I}_{f_1}$  to cut off the UV divergence:

$$\exp \left[ \frac{k^2 - m_a^2}{\Lambda^2} + \frac{(p-k)^2 - m_b^2}{\Lambda^2} + \frac{(k-p_1)^2 - m_c^2}{\Lambda^2} \right], \quad (64)$$

where  $\Lambda$  is the cutoff energy and characterize the effective range of the interaction. In principle, other forms of form factors can also be examined and we find the results are similar to each other.

We present the calculations based on the above two treatments in Fig. 4. In the kinematic region that all the internal particles are close to their mass shells, namely the TS kinematics, these two treatments give nearly identical results since the form factor corrections are nearly unity. In particular, the absorptive part is dominated by the contributions from the TS kinematics. The real part turns out to be more sensitive to the form factor corrections when the internal particles deviate from their mass shells. Similar results are found for the  $f_1(1420)$  since its mass is nearly the same as  $\eta(1440)$  and they share the same TSM. As a result, one can imagine that there should be little difference between these two treatments in the isospin-violating decay of  $\eta(1440)/f_1(1420) \rightarrow 3\pi$  since the main contribution is from the absorptive part in the TS kinematics and the dispersive part would largely cancel out between the charged and neutral loop amplitudes. It is worth noting that the cancellation between the charged and neutral loop amplitudes eventually makes the calculation almost independent of the model uncertainties as explicitly pointed out in Ref. [8]. This should be a direct way to confirm the dominance of the TSM in  $\eta \rightarrow 3\pi$  as a dynamic mechanism.

#### B. Angular distribution analysis

In the numerical calculations, the common coupling constants present in the triangle loops for  $\eta(1440)$  and  $f_1(1420)$  are adopted the same as in Ref. [8], i.e.  $g_{aK\bar{K}} = 3.33$  GeV,  $g_{a\eta\pi} = 2.45$  GeV,  $g_{K^*K\pi}^n = 3.208$ , and  $g_{K^*K\pi}^c = 3.268$ . BES [13] and KLOE [14] give different values for the  $f_0(980)$  coupling, namely,  $g_{f_K\bar{K}} = 4.18$  GeV and  $g_{f\pi\pi} = 1.66$  GeV from BES [13]; and  $g_{f_K\bar{K}} = 5.92$  GeV and  $g_{f\pi\pi} = 2.09$  GeV from KLOE [14]. Similar to the treatment in Ref. [8], contributions from Figs. 1(b) and (2b) are neglected since they are only about 1/10 of Figs. 1(a) and (2a), respectively.

We adopt the mass and width of  $f_1(1420)$  from the PDG [4], i.e.  $m_{f_1(1420)} = 1.4264$  GeV and  $\Gamma_{f_1(1420)} = 54.9$  MeV, but leave the mass and width of  $\eta(1440)$  to be fitted by the experimental data based on the ‘‘one-state’’ assumption. This is reasonable since the  $f_1$  spectrum does not suffer from the ambiguity of possible abundant states in this energy region and as we shall see later that the  $f_0(980)$  angular distribution measured by BESIII [6] only requires a small contribution from the  $f_1(1420)$ .

Taking into account the present datum status, our analysis strategy is as follows: we first fit the BESIII data [6] for the angular distributions of the recoiled photon and  $f_0(980)$  in the decay of  $J/\psi \rightarrow \gamma X$  and  $X \rightarrow f_0(980)\pi^0$ . This allows us to extract the relative strengths between the  $\eta(1440)$  and  $f_1(1420)$  in the isospin violating decays. Then, by applying for the constraint from the  $J/\psi \rightarrow \gamma\eta(1405/1475) \rightarrow \gamma K\bar{K}\pi$  from DM2, MARK III, and BES [4],

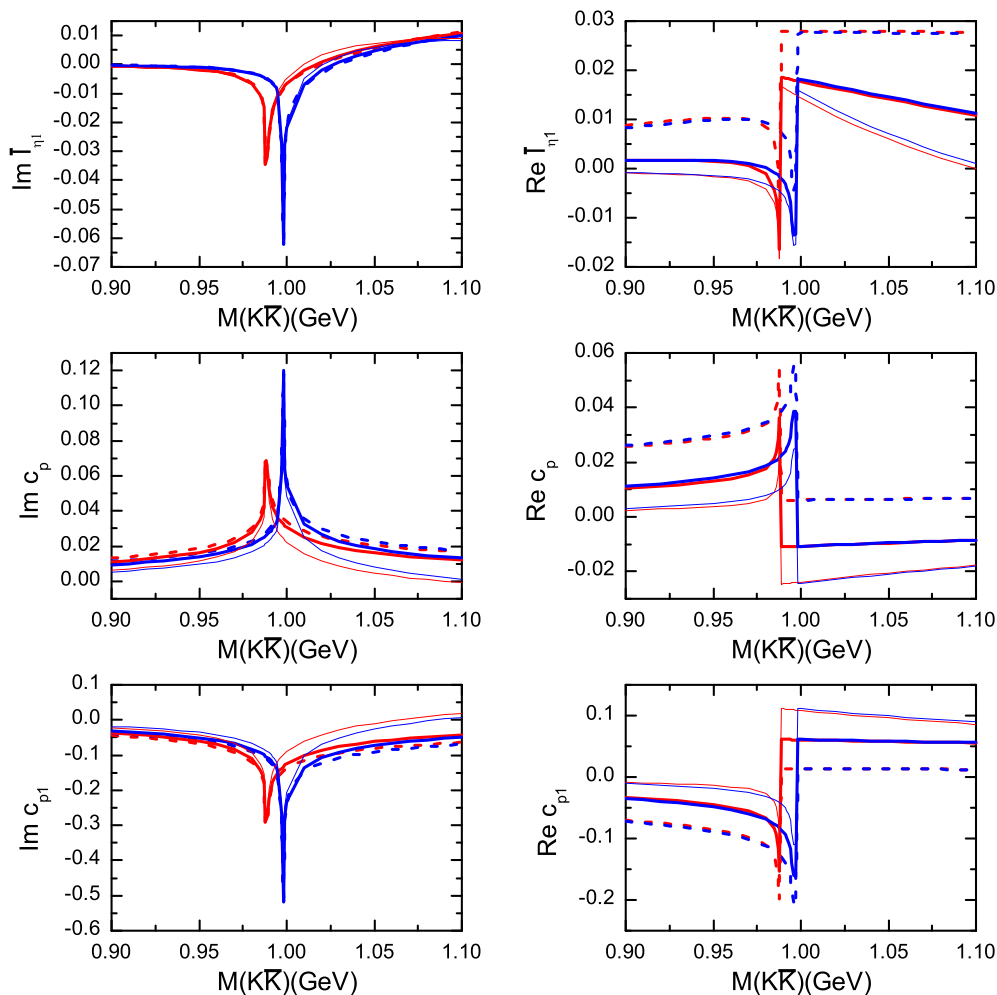


FIG. 4: The imaginary and real parts of the loop integrals in terms of the invariant mass of  $K\bar{K}$  at  $\sqrt{s} = 1.42$  GeV. There are two sets of lines identified by those two spikes which correspond to the charged (lower mass) and neutral (higher mass)  $K\bar{K}$  thresholds. For each set of lines, the thick and thin solid ones represent the results with  $\Lambda = 1.0$  and  $\Lambda = 0.5$  GeV, respectively, while the dashed lines denote the results of *LoopTools* calculation without form factor.

it allows us to determine the absolute differential widths for both  $\eta(1440)$  and  $f_1(1420)$ . We shall compare this with the exclusive fit by  $\eta(1440)$  as shown in Ref. [8]. In the end, we shall output the invariant mass spectra for  $\eta(1440)/f_1(1420) \rightarrow K\bar{K}\pi$ ,  $\eta\pi\pi$  and  $3\pi$ , from which we would expect to observe different lineshapes and peak positions from the same state in different decay channels.

The  $\theta_\gamma$  and  $\theta_{f_0}$  angular distributions of exclusive  $\eta(1440)$  and  $f_1(1420)$  have been analyzed in Ref. [6] as parameterized in Eqs (47)-(48) and (51)-(52). Now we consider the combined contributions from both  $\eta(1440)$  and  $f_1(1420)$  and fit the BESIII data [6] using Eqs. (55)-(56) which can be expressed as

$$\frac{dN}{d\cos\theta_\gamma} = b_\gamma(1 + c\cos^2\theta_\gamma), \quad (65)$$

$$\frac{dN}{d\cos\theta_{f_0}} = b_{f_0}(1 + c_1\cos\theta_{f_0} + c_2\cos^2\theta_{f_0}), \quad (66)$$

where  $b_\gamma$  and  $b_{f_0}$  are the overall normalization factors and

$$c \equiv \frac{1 - 2\alpha_1^2 + 3r_1^2}{1 + 2\alpha_1^2 + 3r_1^2}, \quad c_1 \equiv \frac{4r_1 \cos \phi_r}{\alpha_1^2 + 2r_1^2}, \quad c_2 \equiv \frac{2 - \alpha_1^2}{\alpha_1^2 + 2r_1^2}. \quad (67)$$

We use the CERN program MINUIT to fit the data and the fitting results are demonstrated in Fig. 5. To compare with the results of Ref. [6], we show the  $\chi^2$  values of different fits in Table I. From Fig. 5 we can see that the angular distributions are improved significantly when both  $\eta(1440)$  and  $f_1(1420)$  are included. The apparently asymmetric behavior of the  $\cos \theta_{f_0}$  distribution in Fig. 5 can be well explained as the interference between  $\eta(1440)$  and  $f_1(1420)$ .

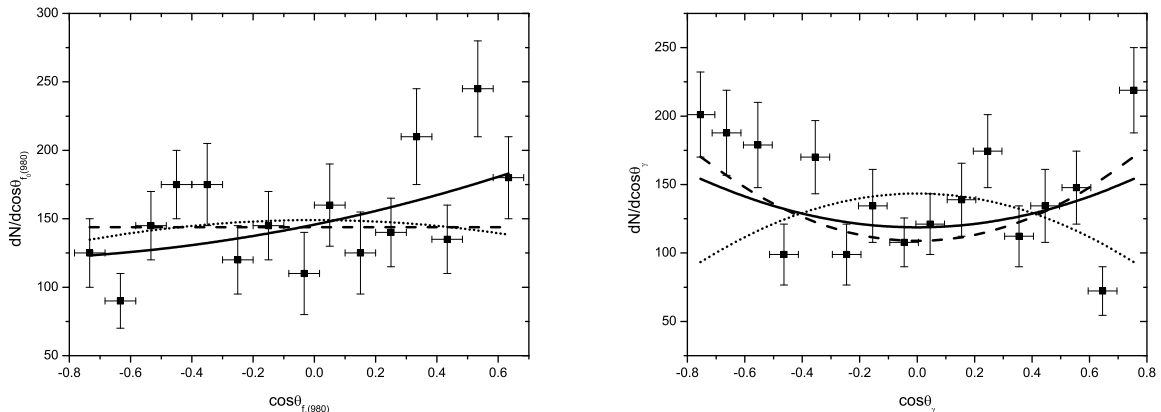


FIG. 5: Fitting results for the  $\cos \theta_{f_0}$  (980) distribution (left panel) and  $\cos \theta_\gamma$  distribution (right panel), respectively. The solid lines are the results considering both  $\eta(1440)$  and  $f_1(1420)$ , while the dashed and dotted lines are the results with exclusive  $\eta(1440)$  or  $f_1(1420)$ , respectively.

TABLE I: The fitting qualities of different fits.

immediate states	$\chi^2/d.o.f$ for $\cos \theta_\gamma$	$\chi^2/d.o.f$ for $\cos \theta_{f_0}$
$\eta(1440)$	40.2/15	26.8/14
$f_1(1420)$	59.0/15	26.4/13
$\eta(1440)$ and $f_1(1420)$	38.3/14	19.8/12

The fitted parameters are as follows:

$$b_\gamma = 118.5 \pm 8.8, \quad c = 0.538 \pm 0.312, \quad (68)$$

from the  $\theta_\gamma$  distribution and

$$b_{f_0} = 145.7 \pm 10.7, \quad c_1 = 0.314 \pm 0.128, \quad c_2 = 0.141 \pm 0.317, \quad (69)$$

for  $\theta_{f_0}$ . By solving Eq. (67), we obtain

$$\alpha_1^2 = 1.197 \pm 1.090, \quad r_1 = 1.50 \pm 0.89, \quad \phi_r = \pm(1.27 \pm 0.20), \quad (70)$$

which will allow us to extract the coupling constants for  $f_1(1420)$ , i.e.  $g_{f_1(1420)K^*K}$ ,  $g_1$ , and  $g_2$ . Coupling  $g_{f_1(1420)K^*K}$  can be directly obtained from the width of  $f_1(1420)$  [4] by assuming that  $K\bar{K}\pi$  channel is dominant;  $g_{\psi\gamma\eta(1440)}/g_1$  is related to the fitted  $r_1$ ; and  $g_2/g_1$  is related to the fitted  $\alpha_1$ .

The fitted parameters of  $\eta(1440)$  are  $m_{\eta(1440)} = 1.42$  GeV,  $\Gamma_{\eta(1440)} = 67$  MeV. The extracted couplings are listed in Table II. There are two solutions for the ratio of the  $D$ -wave coupling to  $S$ -wave coupling  $g_2/g_1$ , i.e. the value  $-0.179$  indicates the  $S$ -wave dominant, while the value  $0.970$  indicates the  $D$ -wave dominant. The present precision of the experimental data seems impossible to distinguish these two solutions. From our fit we find that the ratio of  $f_1(1420)$  to  $\eta(1440)$  in the  $K\bar{K}\pi$  channel is about 17.3%.

TABLE II: Couplings extracted from the angular distribution analysis.

$g_{\eta(1440)K^*K}$	3.638
$g_{J/\psi\gamma\eta(1440)}(\text{GeV}^{-1})$	$(1.59 \pm 0.32) \times 10^{-3}$
$g_{f_1K^*K}(\text{GeV})$	$2.282 \pm 0.054$
$g_1$	$(4.4 \pm 2.7) \times 10^{-4}$
$g_2/g_1(\text{GeV}^{-2})$	$-0.179_{-0.219}^{+0.403}$ or $0.970_{-0.403}^{+0.219}$
$\frac{\Gamma(J/\psi \rightarrow \gamma f_1 \rightarrow \gamma K \bar{K} \pi)}{\Gamma(J/\psi \rightarrow \gamma \eta(1440) \rightarrow \gamma K \bar{K} \pi)}$	$(17.3 \pm 23.4)\%$ or $(17.1 \pm 23.1)\%$

With these couplings, we can predict the corresponding spectra and ratios for  $J/\psi \rightarrow \gamma f_1(1420)$  with  $f_1(1420) \rightarrow K\bar{K}\pi$ ,  $\pi^+\pi^-\pi^0$  and  $\eta\pi^0\pi^0$  as shown in Fig. 6 and Table III. The results obtained by those two values of  $g_2/g_1$  are almost identical as demonstrated in Fig. 6(a) for the  $K\bar{K}\pi$  channel. So, in other channels we only show the results with  $g_2/g_1 = -0.179$ . The main features of spectra and ratios are similar to those of  $\eta(1440)$ .

In the  $\pi^+\pi^-\pi^0$  channel, the results of KLOE are larger than those of BESIII by a factor of about 1.11 due to the difference of  $g_{f_1K\bar{K}}$  and  $g_{f_1\pi\pi}$  extracted from these two experiments as mentioned earlier. Meanwhile, it shows that the partial width (or branching ratio) is insensitive to the form factor cut-off energy. This feature has been discussed earlier and it is because that the model uncertainties will be largely constrained by the cancellation between the charged and neutral loop amplitudes. Nevertheless, the dominant contributions to the isospin-violating decays are from the TS kinematics where the form factor effects are rather small.

In the  $\eta\pi^0\pi^0$  channel, the results are sensitive to the integration methods and cut-off energies due to the contributions from the dispersive part in the loop integrals. When varying the cut-off  $\Lambda$  from 1.0 GeV to 0.5 GeV, the results change about 31%.

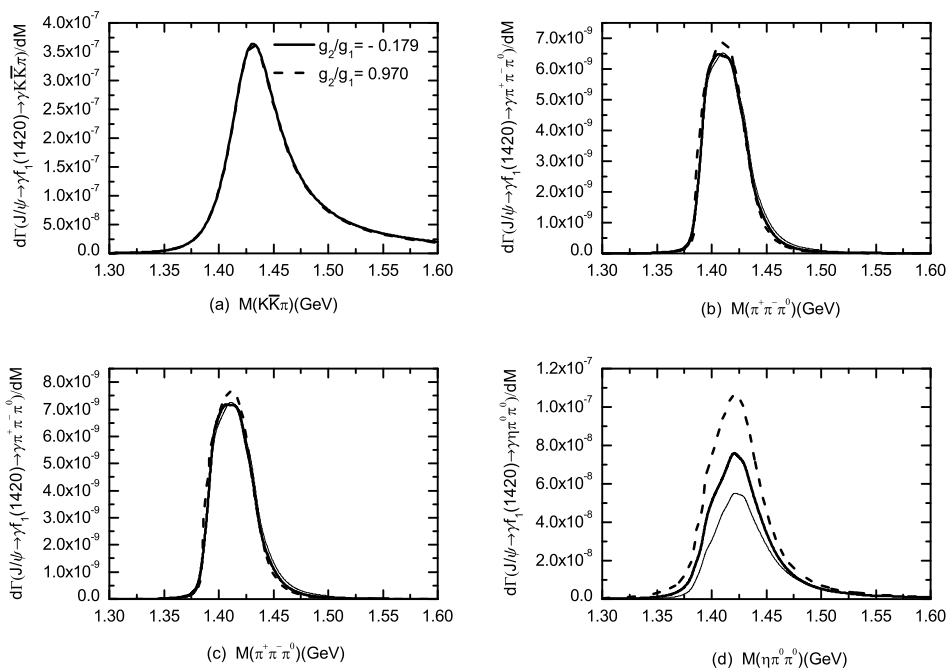


FIG. 6: Predictions for the spectra  $d\Gamma(J/\psi \rightarrow \gamma f_1(1420) \rightarrow \gamma ABC)/d\sqrt{s}$ . Figure (a) is for the  $K\bar{K}\pi$  channel where the solid and dashed line denote results with different values of  $g_2/g_1$ . Figures (b) and (c) are for the  $\pi^+\pi^-\pi^0$  channel with  $g_{f_0K\bar{K}}$  and  $g_{f_0\pi\pi}$  determined by the BES and KLOE data, respectively, and (d) for the  $\eta\pi^0\pi^0$  channel. The thick and thin solid lines in Figures (b-d) correspond to the results with  $\Lambda = 1.0$  and  $0.5$  GeV, respectively, while the dashed lines denote the results by the *LoopTools* calculation without form factor.

As we expect that the TSM appears to be more significant in  $f_1(1420)$  than in  $\eta(1440)$  since the coupling  $f_1(1420) \rightarrow K^*\bar{K} + c.c.$  is in a relative  $S$  wave, while  $\eta(1440) \rightarrow K^*\bar{K} + c.c.$  is in a  $P$  wave. Taking the results with  $\Lambda = 1.0$  GeV

TABLE III: The extracted results for  $f_1(1420)$ , where  $\Gamma_{ABC} \equiv \Gamma(J/\psi \rightarrow \gamma f_1(1420) \rightarrow \gamma ABC)$  and  $R_{ABC} \equiv \Gamma_{ABC}/\Gamma_{K\bar{K}\pi}$ .

coupling		$g_2/g_1 = -0.179 \text{ GeV}^{-2}$		$g_2/g_1 = 0.970 \text{ GeV}^{-2}$	
channel		$\Gamma(\text{keV})$	$R$	$\Gamma(\text{keV})$	$R$
$K\bar{K}\pi$		$2.67 \times 10^{-2}$	1	$2.63 \times 10^{-2}$	1
$\pi^+\pi^-\pi^0(\text{BES})$	LoopTool	$3.18 \times 10^{-4}$	1.19%	$3.18 \times 10^{-4}$	1.21%
	$\Lambda = 1.0 \text{ GeV}$	$3.06 \times 10^{-4}$	1.15%	$3.06 \times 10^{-4}$	1.16%
	$\Lambda = 0.5 \text{ GeV}$	$3.11 \times 10^{-4}$	1.17%	$3.11 \times 10^{-4}$	1.18%
$\pi^+\pi^-\pi^0(\text{KLOE})$	LoopTool	$3.54 \times 10^{-4}$	1.33%	$3.54 \times 10^{-4}$	1.34%
	$\Lambda = 1.0 \text{ GeV}$	$3.40 \times 10^{-4}$	1.27%	$3.89 \times 10^{-4}$	1.29%
	$\Lambda = 0.5 \text{ GeV}$	$3.45 \times 10^{-4}$	1.29%	$3.45 \times 10^{-4}$	1.31%
$\eta\pi^0\pi^0$	LoopTool	$6.78 \times 10^{-3}$	25.4%	$6.74 \times 10^{-3}$	25.6%
	$\Lambda = 1.0 \text{ GeV}$	$4.68 \times 10^{-3}$	17.5%	$4.68 \times 10^{-3}$	17.8%
	$\Lambda = 0.5 \text{ GeV}$	$3.24 \times 10^{-3}$	12.1%	$3.24 \times 10^{-3}$	12.3%

as an example, the ratio of  $\pi^+\pi^-\pi^0$  to  $K\bar{K}\pi$  is 1.27% in  $f_1(1420)$ , while in  $\eta(1440)$  the ratio is 0.762%. The ratio of  $\eta\pi^0\pi^0$  to  $K\bar{K}\pi$  is 17.5% in  $f_1(1420)$ , while in  $\eta(1440)$  the ratio is 6.61%. The contributions from the  $f_1(1420)$  also affects the peak position as demonstrated in the next Subsection.

### C. Invariant mass spectra including both $\eta(1440)$ and $f_1(1420)$

With the parameters fixed as the above, we compare the spectra and ratios with experiment [6] in Fig. 7 and Table IV where both  $\eta(1440)$  and  $f_1(1420)$  are included. The main features are consistent with Ref. [8] where only  $\eta(1440)$  was considered.

It shows that the contribution of  $f_1(1420)$  is much smaller than that of  $\eta(1440)$  in  $J/\psi \rightarrow \gamma\eta(1440)/f_1(1420) \rightarrow \gamma K\bar{K}\pi$ . However, one should be reminded that this is largely due to the suppressed coupling for  $J/\psi \rightarrow \gamma f_1(1420)$ . In contrast, the contribution from the  $f_1(1420)$  is relatively enhanced in the  $\eta\pi^0\pi^0$  channel than in  $K\bar{K}\pi$  because of the TSM. The most interesting scenario is that the lineshapes of the invariant mass spectra for the  $K\bar{K}\pi$ ,  $\eta\pi^0\pi^0$  and  $\pi^0\pi^+\pi^-$  decays are very different from each other due to the presence of the TSM in the last two processes. Also, the interferences of the TSM have led to the shifts of peak positions in those three channels which describe the experimental data consistently. Such a phenomenon retains even with contributions from  $\eta(1440)$  exclusively as found in Ref. [8].

For the isospin-violating channel of  $\eta(1440)/f_1(1420) \rightarrow 3\pi$ , the observation of the narrow  $f_0(980)$  in the  $\pi\pi$  spectrum can be regarded as a signature of the TSM. As being shown in Ref. [8], the narrow peak is located between the charged and neutral  $K\bar{K}$  thresholds as a residual contribution due to the isospin violation. The mass difference between the charged and neutral kaons gives rise to the nonvanishing amplitudes between the  $K^+K^-$  and  $K^0\bar{K}^0$  thresholds which has been a crucial mechanism for the  $a_0(980)$  and  $f_0(980)$  mixing. Beyond this scenario, what we show here and in Ref. [8] is that the TSM can further dominantly enhance the  $f_0(980)$  production in  $\eta(1440)/f_1(1420) \rightarrow 3\pi$  which eventually explains the anomalously large isospin violations.

As listed in Table IV, we can see that the ratios of  $\pi^+\pi^-\pi^0$  and  $\eta\pi^0\pi^0$  to  $K\bar{K}\pi$  agree well with experiment. Meanwhile, one also notices that the relative contributions from  $f_1(1420)$  to  $\eta(1440)$  are quite different in different channels as we discussed in Fig. 7. Namely, the relative strength of  $f_1(1420)$  to  $\eta(1440)$  turns out to be more significant in the  $\eta\pi^0\pi^0$  channel than in the  $K\bar{K}\pi$ . It is because the  $S$ -wave coupling of  $K^*K$  to  $f_1(1420)$  would allow a relatively enhanced contributions from the TSM in  $J/\psi \rightarrow \gamma f_1(1420) \rightarrow \gamma\eta\pi^0\pi^0$  than  $\eta(1440)$ .

In Table V we present the  $\eta(1440)$  and  $f_1(1420)$  peak positions extracted in those three decay channels. Due to the contributions from the TSM, the peak positions are shifted differently. It shows that the exclusive results for  $\eta(1440)$  and  $f_1(1420)$  respectively or the results with their combined contributions have a similar feature. Namely, the largest peak mass can be seen in the  $K\bar{K}\pi$  channel, while the smallest one is the  $3\pi$  channel. This qualitative pattern fits well the experimental observations in these three decay channels.

Because of the TSM, the peak positions in both  $\eta\pi\pi$  and  $3\pi$  channels would move towards the  $K^*\bar{K} + c.c.$  threshold which is about 1.39 GeV. The more significant the TSM contribution is, the larger the peak position shift would be. As a result of the TSM dominance in the  $\pi^+\pi^-\pi^0$  channel, the peak position observed in the  $\pi^+\pi^-\pi^0$  channel has a lower value than that in the  $\eta\pi^0\pi^0$  channel. The importance of the TSM suggests that a partial wave analysis including the TSM is necessary. Such a mechanism may also have significant interferences with the background. As

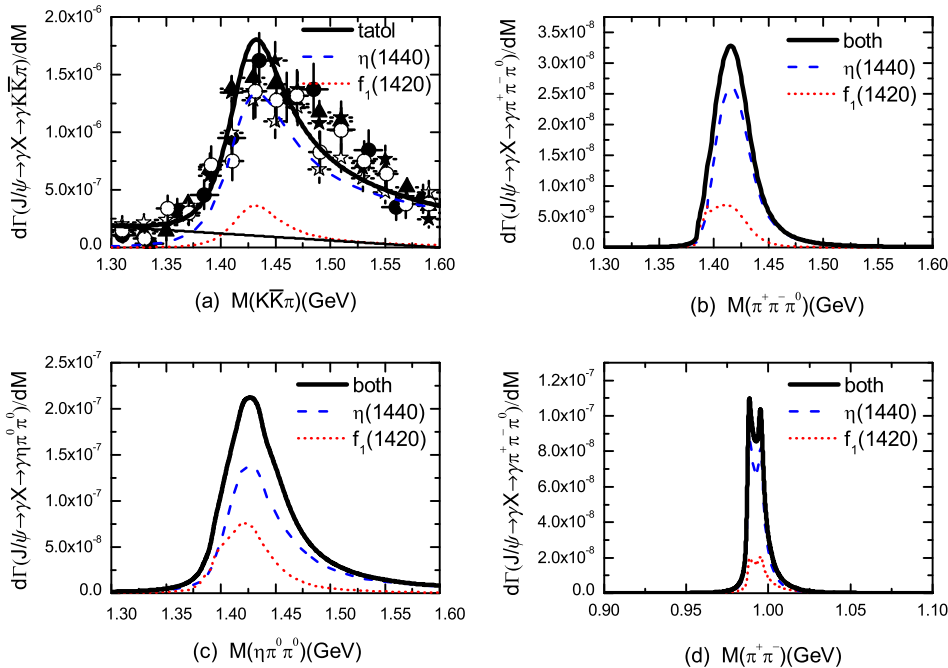


FIG. 7: The spectra  $d\Gamma(J/\psi \rightarrow \gamma X \rightarrow \gamma ABC)/d\sqrt{s}$  including both  $\eta(1440)$  and  $f_1(1420)$ . In the  $K\bar{K}\pi$  channel, we also show the experimental data, i.e. the solid triangles, solid circles, hollow circles, solid pentacles and hollow pentacles from MARK III( $K_S^0 K^\pm \pi^\mp$ ) [15], BES( $K_S^0 K^\pm \pi^\mp$ ) [16], BES( $K^\pm K^\mp \pi^0$ ) [17], DM2( $K_S^0 K^\pm \pi^\mp$ ) [18], and DM2( $K^+ K^- \pi^0$ ) [18], respectively. The thin line in Fig. (a) is the background. In the  $\pi^+ \pi^- \pi^0$  and  $\pi^+ \pi^-$  channels, we show the results given by the *LoopTools* calculation with  $g_{f_0 KK}$  and  $g_{f_0 \pi\pi}$  determined by BES. In the  $\eta\pi^0\pi^0$  channel, we choose the results with  $\Lambda = 1.0$  GeV.

TABLE IV: The combined results for  $R_{ABC} = \Gamma(J/\psi \rightarrow \gamma X \rightarrow \gamma ABC)/\Gamma(J/\psi \rightarrow \gamma X \rightarrow \gamma K\bar{K}\pi)$  including both  $\eta(1440)$  and  $f_1(1420)$ . The experimental data [6, 16, 19, 20] are also listed. For  $f_1(1420)$  we adopt  $g_2/g_1 = -0.179$ .

		R	
channel		Theory	Expt.
$K\bar{K}\pi$		1	1
LoopTool		0.781%	
$\pi^+ \pi^- \pi^0$ (BES)	$\Lambda = 1.0$ GeV	0.746%	$(0.90 \pm 0.39)\%$
	$\Lambda = 0.5$ GeV	0.752%	
LoopTool		0.878%	
$\pi^+ \pi^- \pi^0$ (KLOE)	$\Lambda = 1.0$ GeV	0.837%	$(0.90 \pm 0.39)\%$
	$\Lambda = 0.5$ GeV	0.843%	
LoopTool		23.7%	
$\eta\pi^0\pi^0$	$\Lambda = 1.0$ GeV	8.22%	$(7.8 \pm 4.6)\%$
	$\Lambda = 0.5$ GeV	5.28%	

a consequence, it will lead to different lineshapes for the  $\eta(1440)$  in different production channels. For instance, the peak position of the  $\eta(1440)$  in  $J/\psi \rightarrow \gamma\eta\pi\pi$  is slightly different from that in  $J/\psi \rightarrow \omega\eta\pi\pi$  [21]. Note that the results of Ref. [21] are given by simple Breit-Wigner fit instead of partial wave analysis. Further detailed analysis of this channel using partial wave analysis should include the TSM as an important underlying dynamics in order to extract the correct pole position for the  $\eta(1440)$ .

With  $m_{\eta(1440)} = 1.42$  GeV and  $m_{f_1(1420)} = 1.4264$  GeV, we find that the peak position shifts in the  $f_1(1420)$  decays are larger than in  $\eta(1440)$ . The reason again is because of the relative  $S$ -wave coupling for  $f_1(1420) \rightarrow K^* \bar{K} + c.c.$

When combining  $\eta(1440)$  and  $f_1(1420)$  together, the largest peak position shift that we can achieve is about 24 MeV, which supports our one-state assumption. Namely, the  $\eta(1405)$  and  $\eta(1475)$  may be just one state in different channels.

TABLE V: Peak positions in different channels.

peak position (GeV)	$K\bar{K}\pi$	$\pi^+\pi^-\pi^0$	$\eta\pi^0\pi^0$
$\eta(1440)$	1.433	1.416	1.426
$f_1(1420)$	1.431	1.411	1.422
$\eta(1440) + f_1(1420)$	1.432	1.415	1.425

#### D. Radiative decays of $\eta(1405/1475)$

Our proposal that  $\eta(1405)$  and  $\eta(1475)$  are the same state would have an explicit consequence in the description of the radiative decays of  $\eta(1405/1475) \rightarrow \gamma V$ , where  $V$  stands for the light vector mesons  $\phi$ ,  $\rho^0$  and  $\omega$ . In the one-state assumption,  $\eta(1440)$  would be the SU(3) flavor partner of  $\eta(1295)$  as the first radial excitation states of  $\eta$  and  $\eta'$ . In Ref. [5], it was commented that by assigning the  $\eta(1475)$  to the SU(3) partner of  $\eta(1295)$  as the  $s\bar{s}$  dominant state would not be able to explain why the observed branching ratios  $BR(\eta(1475) \rightarrow \gamma\rho^0)$  is larger than  $BR(\eta(1475) \rightarrow \gamma\phi)$ . Also, it was commented that the observation that the much stronger production rate of  $J/\psi \rightarrow \gamma\eta(1405/1475)$  than  $J/\psi \rightarrow \gamma\eta(1295)$  seemed not be obvious taking into account the above question. However, in this Subsection, we shall show that the experimental observations can be self-consistently understood by treating  $\eta(1440)$  and  $\eta(1295)$  as the SU(3) flavor partners. This can be explicitly demonstrated as the following:

By assigning  $\eta(1295)$  and  $\eta(1440)$  as the first radial excitation of  $\eta$  and  $\eta'$ , we can organize them as the following mixtures between  $n\bar{n} \equiv (u\bar{u} + d\bar{d})/\sqrt{2}$  and  $s\bar{s}$ :

$$\begin{aligned}\eta(1295) &= \cos\alpha n\bar{n} - \sin\alpha s\bar{s} \\ \eta(1440) &= \sin\alpha n\bar{n} + \cos\alpha s\bar{s},\end{aligned}\tag{71}$$

where  $\alpha$  is the mixing angle.

In the  $J/\psi$  radiative decays, it is a good approximation that the photon is radiated by the charm (anti-)quark, and the light  $q\bar{q}$  of  $0^{-+}$  is produced by the gluon radiation. By defining the production strength for the  $q\bar{q}$  of  $0^{-+}$  as the following:

$$g_0 \equiv \langle q\bar{q} | \hat{H} | J/\psi, \gamma \rangle,\tag{72}$$

one can express the production amplitudes for  $\eta(1295)$  and  $\eta(1440)$  as

$$\begin{aligned}\mathcal{M}(\eta(1295)) &= (\sqrt{2}\cos\alpha - R\sin\alpha)g_0, \\ \mathcal{M}(\eta(1440)) &= (\sqrt{2}\sin\alpha + R\cos\alpha)g_0,\end{aligned}\tag{73}$$

where  $R \equiv \langle s\bar{s} | \hat{H} | J/\psi, \gamma \rangle / g_0$  is an SU(3) flavor symmetry breaking factor, and one can simply set it to be unity as a leading approximation. It can be easily seen that a proper value for the mixing angle  $\alpha$  in the first quadrant would lead to a much suppressed b.r. for  $J/\psi \rightarrow \gamma\eta(1295)$  than for  $J/\psi \rightarrow \gamma\eta(1440)$ . The value of  $\alpha$  can be determined by the b.r.s measured for these two channels. For instance, if one requires that  $B.R.(J/\psi \rightarrow \gamma\eta(1440)) / B.R.(J/\psi \rightarrow \gamma\eta(1295)) \simeq 10$ , namely, the production of  $\eta(1440)$  is about one order of magnitude larger than  $\eta(1295)$ , one would have

$$\frac{B.R.(J/\psi \rightarrow \gamma\eta(1440))}{B.R.(J/\psi \rightarrow \gamma\eta(1295))} = \left(\frac{q_{\eta(1440)}}{q_{\eta(1295)}}\right)^3 \left(\frac{\sqrt{2}\sin\alpha + R\cos\alpha}{\sqrt{2}\cos\alpha - R\sin\alpha}\right)^2 \simeq 10,\tag{74}$$

where  $q_{\eta(1440)}$  and  $q_{\eta(1295)}$  are three momenta of the pseudoscalars in the  $J/\psi$  rest frame, respectively. with  $R \equiv 1$ , one has  $\alpha \simeq 38^\circ$ . Such a mixing scenario will have explicit predictions for the radiative decays of  $\eta(1440) \rightarrow \phi\gamma$ ,  $\rho^0\gamma$  and  $\omega\gamma$ .

Since  $\phi$  and  $\omega$  are nearly ideally mixed to each other and  $\rho^0$  has isospin-1, we adopt the flavor wavefunctions,  $\phi = s\bar{s}$  and  $\omega = n\bar{n}$ , and  $\rho^0 = (u\bar{u} - d\bar{d})/\sqrt{2}$ . The  $\eta(1440)$  radiative decays are via M1 transitions where the quark spin will be flipped by the magnetic interaction. A standard operator in the quark model can be written as

$$\hat{H}_{em} \equiv \langle \phi_A \chi_S | \sum_i^2 e_i \mu_i \vec{\sigma}_i \cdot \vec{\epsilon}_\gamma | \phi_S \chi_A \rangle,\tag{75}$$



where  $\mu_i \equiv e/2m_i$  is the magnetic moment of the  $i$ th quark, and  $|\phi_S\chi_A\rangle$  and  $|\phi_A\chi_S\rangle$  are the flavor-spin wavefunctions for  $\eta(1440)$  and vector meson, respectively. The subscriptions  $S$  and  $A$  means that the corresponding wavefunctions are symmetric or anti-symmetric under the exchange of the first and second quark (anti-quark). The flavor and spin wavefunctions are defined in a standard way as the following:

$$\begin{aligned}\phi_S(s\bar{s}) &\equiv (s\bar{s} + \bar{s}s)/\sqrt{2}, \\ \phi_S(n\bar{n}) &\equiv (n\bar{n} + \bar{n}n)/\sqrt{2}, \\ \chi_A &\equiv (\uparrow\downarrow - \downarrow\uparrow)/\sqrt{2}\end{aligned}\quad (76)$$

for the pseudoscalar state, and

$$\begin{aligned}\phi_A(\phi) &\equiv (s\bar{s} - \bar{s}s)/\sqrt{2}, \\ \phi_A(\rho^0) &\equiv ((u\bar{u} - \bar{u}u) - (d\bar{d} - \bar{d}d))/2, \\ \phi_A(\omega) &\equiv ((u\bar{u} - \bar{u}u) + (d\bar{d} - \bar{d}d))/2, \\ \chi_S &\equiv \uparrow\uparrow, \downarrow\downarrow, (\uparrow\downarrow + \downarrow\uparrow)/\sqrt{2},\end{aligned}\quad (77)$$

for the vectors.

One can easily work out the flavor-spin couplings for those three channels as follows:

$$\begin{aligned}h_{\phi\gamma} &= -\frac{e}{3m_s} \cos \alpha, \\ h_{\rho^0\gamma} &= \frac{e}{2m_q} \sin \alpha, \\ h_{\omega\gamma} &= \frac{e}{6m_q} \sin \alpha,\end{aligned}\quad (78)$$

where  $m_q = m_u = m_d$  and  $m_s \simeq 5m_q/3$ . Apart from the spacial form factor and phase space factor in a  $P$  wave, the b.r. fraction among these decay channels are then

$$B.R.(\gamma\phi) : B.R.(\gamma\rho^0) : B.R.(\gamma\omega) \simeq \frac{\cos^2 \alpha}{25} : \frac{\sin^2 \alpha}{4} : \frac{\sin^2 \alpha}{36} . \quad (79)$$

For a proper value of  $\alpha$  in the first quadrant, the decay of  $\eta(1440) \rightarrow \gamma\rho^0$  would be dominant. To be consistent with the production of  $\eta(1440)$  and  $\eta(1295)$  in the  $J/\psi$  radiative decays, i.e.  $\alpha \simeq 38^\circ$ , one obtains  $B.R.(\gamma\phi) : B.R.(\gamma\rho^0) : B.R.(\gamma\omega) \simeq 1 : 3.8 : 0.42$ .

In brief, given a proper mixing angle between the  $\eta(1295)$  and  $\eta(1440)$  as the first radial excitation states of  $\eta$  and  $\eta'$ , the theoretical interpretation of the  $\eta(1405/1475)$  as a single state of  $\eta(1440)$  does not obviously conflict with the so far available experimental data at all. The misunderstanding that the branching ratio of  $\eta(1475) \rightarrow \gamma\phi$  should be larger than that of  $\eta(1475) \rightarrow \gamma\rho^0$  if  $\eta(1475)$  is the higher mass partner of  $\eta(1295)$  is not necessary at all due to the suppression of the quark masses in the M1 transition. This point, unfortunately, has not been realized in earlier analyses.

#### IV. SUMMARY

In summary, we have made a systematic analysis of the correlated processes  $J/\psi \rightarrow \gamma\eta(1440)/f_1(1420)$  with  $\eta(1440)/f_1(1420) \rightarrow K\bar{K}\pi$ ,  $\eta\pi\pi$  and  $3\pi$ , where the role played by the TSM is clarified. Our combined analysis including  $\eta(1440)$  and  $f_1(1420)$  agrees well with the experiment data, and provides an overall description of the processes  $J/\psi \rightarrow \gamma X$  with  $X \rightarrow K\bar{K}\pi$ ,  $\eta\pi^0\pi^0$ , and  $\pi^+\pi^-\pi^0$ . In particular, we show that the inclusion of the  $f_1(1420)$  can improve the description of the  $f_0(980)\pi^0$  angular distribution significantly, although the contribution from  $f_1(1420)$  is much smaller than  $\eta(1440)$ . By fitting the BESIII data for  $J/\psi \rightarrow \gamma X \rightarrow \gamma f_0(980)\pi^0$ , we extract the coupling parameters of  $f_1(1420)$ . It allows us to estimate that the ratio of  $f_1(1420)$  to  $\eta(1440)$  in the  $K\bar{K}\pi$  channel is about 17.3%. This does not change the results of the previous work [8] in which we assumed that  $\eta(1440)$  was the only contributing state as treated by the BESIII. We also show that  $f_1(1420)$  can contribute some percentages to the narrow peak of  $f_0(980) \rightarrow \pi\pi$  via the TSM.

We emphasize that the dynamic feature of the TSM can be recognized by the strong narrow peak observed in the  $3\pi$  channel with the anomalously large isospin violations. Moreover, it leads to the obvious peak position shifts for the same  $\eta(1440)$  or  $f_1(1420)$  state in different decay channels, which may suggest that the  $\eta(1405)$  and  $\eta(1475)$  are actually the same state. So far, such a one-state prescription seems not to have a conflict with existing experimental data. This may shed a light on the long-standing puzzling question on the nature of  $\eta(1405)$  and  $\eta(1475)$  in the literature.



## V. ACKNOWLEDGMENTS

Useful discussions with X.-H. Liu, X.-Y. Shen, and Z. Wu are acknowledged. This work is supported, in part, by the National Natural Science Foundation of China (Grant Nos. 11035006 and 11121092), DFG and NSFC (CRC 110), Chinese Academy of Sciences (KJ CX2-EW-N01), Ministry of Science and Technology of China (2009CB825200), and U.S. Department of Energy (Contract No. DE-AC02-06CH11357).

- 
- [1] M. Ablikim et al. (BES Collaboration), *Phys.Rev.Lett.* **95**, 262001 (2005), hep-ex/0508025.
  - [2] M. Ablikim et al. (BESIII Collaboration), *Phys.Rev.Lett.* **106**, 072002 (2011), 1012.3510.
  - [3] J.-S. Yu, Z.-F. Sun, X. Liu, and Q. Zhao, *Phys.Rev.* **D83**, 114007 (2011), 1104.3064.
  - [4] K. Nakamura et al. (Particle Data Group), *J.Phys.G* **G37**, 075021 (2010).
  - [5] E. Klempt and A. Zaitsev, *Phys.Rept.* **454**, 1 (2007), 0708.4016.
  - [6] M. Ablikim et al. (BESIII Collaboration), *Phys.Rev.Lett.* **108**, 182001 (2012), 1201.2737.
  - [7] M. Ablikim et al. (BES III Collaboration), *Phys.Rev.* **D83**, 032003 (2011), 1012.5131.
  - [8] J.-J. Wu, X.-H. Liu, Q. Zhao, and B.-S. Zou, *Phys.Rev.Lett.* **108**, 081803 (2012), 1108.3772.
  - [9] F. Aceti, W. Liang, E. Oset, J. Wu, and B. Zou (2012), 1209.6507.
  - [10] B. Zou and D. Bugg, *Eur.Phys.J.* **A16**, 537 (2003), hep-ph/0211457.
  - [11] S. Chung, *Phys.Rev.* **D57**, 431 (1998).
  - [12] X.-G. Wu and Q. Zhao, *Phys.Rev.* **D85**, 034040 (2012), 1111.4002.
  - [13] M. Ablikim et al. (BES Collaboration), *Phys.Lett.* **B607**, 243 (2005), hep-ex/0411001.
  - [14] A. Aloisio et al. (KLOE Collaboration), *Phys.Lett.* **B537**, 21 (2002), hep-ex/0204013.
  - [15] Z. Bai et al. (MARK-III Collaboration), *Phys.Rev.Lett.* **65**, 2507 (1990).
  - [16] J. Bai et al. (BES Collaboration), *Phys.Lett.* **B476**, 25 (2000), hep-ex/0002007.
  - [17] J. Bai et al. (BES Collaboration), *Phys.Lett.* **B440**, 217 (1998).
  - [18] J. Augustin et al. (DM2 Collaboration), *Phys.Rev.* **D42**, 10 (1990).
  - [19] J. Bai et al. (BES Collaboration), *Phys.Lett.* **B446**, 356 (1999).
  - [20] H.-B. Li (BESIII Collaboration) (2011), 1108.5789.
  - [21] M. Ablikim et al. (BESIII Collaboration), *Phys.Rev.Lett.* **107**, 182001 (2011), 1107.1806.